JOURNAL OF GEOPHYSICAL RESEARCH, VOL. 111, E12003, doi:10.1029/2006JE002720, 2006

Exponential sum absorption coefficients of phosphine from 2750 to 3550 cm^{-1} for application to radiative transfer analyses on Jupiter and Saturn

T. Temma,[1] K. H. Baines,[1] R. A. H. Butler,[1,2] L. R. Brown,[1] L. Sagui,[3] and I. Kleiner[3]

Received 23 March 2006; revised 6 July 2006; accepted 25 July 2006; published 8 December 2006.

[1] PH_3 exponential sum k coefficients were computed between 2750 and 3550 cm^{-1} (2.82–3.64 μm), in view of future application to radiative transfer analyses of Jupiter and Saturn in a phosphine absorption band near 3 μm. The temperature and pressure of this data set cover the ranges from 80 to 350 K and from 10^{-3} to 10^{1} bars, respectively. Transmission uncertainty incurred by the use of the k coefficients is smaller than a few percent as long as the radiation is confined above an altitude of a few bars in the giant planets. In spectral regions of weak absorption at high pressures close to 10 bars, contributions from far wings of strong absorption lines must be carefully taken into account. Our data set helps map the three-dimensional distribution of PH_3 on the giant planets, revealing their global atmospheric dynamics extending down to the deep interior. The complete k coefficient data set of this work is available at the Web site of the NASA Planetary Data System Atmospheres Node.

Citation: Temma, T., K. H. Baines, R. A. H. Butler, L. R. Brown, L. Sagui, and I. Kleiner (2006), Exponential sum absorption coefficients of phosphine from 2750 to 3550 cm^{-1} for application to radiative transfer analyses on Jupiter and Saturn, *J. Geophys. Res.*, *111*, E12003, doi:10.1029/2006JE002720.

1. Introduction

[2] Phosphine (PH_3) is a trace element of great interest in giant planet research. Since it is a disequilibrium species in the upper atmosphere of Jupiter and Saturn, the presence of its spectral features in observed spectra indicates constant supply of the molecule from the deep planetary interior. Accordingly, the horizontal variation in vertical PH_3 concentration profiles suggests horizontal distribution of convective activities in giant planets, with more vigorous convection within regions of higher PH_3 abundance at high altitudes.

[3] Evidence of PH_3 on Jupiter was first reported by *Ridgway* [1974] and *Ridgway et al.* [1976] from their 10-μm observation, and further confirmed by the 5-μm observation of *Larson et al.* [1977]. Since then, observations of PH_3 on Jupiter were done mainly over 5–10 μm from the ground, airplane, and Voyager and Galileo spacecraft [*Kunde et al.*, 1982; *Bjoraker et al.*, 1986; *Carlson et al.*, 1993; *Irwin et al.*, 1998]. They determined a PH_3 volume mixing ratio of $\sim 7 \times 10^{-7}$ in the deep Jovian troposphere, and a PH_3 fractional scale height of 0.27–0.30 above the 1-bar level in the 5–13°N latitude region. The newest 10-μm spectrum measurements by the Cassini spacecraft detected significant latitudinal variations in the PH_3 abundance in the deep Jovian atmosphere, hinting at enhancement in PH_3 at the northern edge of the Great Red Spot [*Irwin et al.*, 2004].

[4] Tentative evidence of PH_3 on Saturn was first found by *Gillett and Forrest* [1974] and then by *Bregman et al.* [1975] in Saturn's 10-μm spectrum. Their findings were reinforced by the midinfrared observations of *Larson et al.* [1980]. Thanks to the subsequent studies of Saturn's 5–10-μm spectrum by *Tokunaga et al.* [1980], *Courtin et al.* [1984], *Noll and Larson* [1990], and *Orton et al.* [2000], it is now established that Saturn's PH_3 volume mixing ratio is 2–10 times larger than that of Jupiter [*Atreya et al.*, 1999, 2003; *Encrenaz* 2004]. Recently, some interesting latitudinal variations in PH_3 absorption on Saturn were discovered near 3 μm in the data set of the Visible and Infrared Mapping Spectrometer (VIMS) onboard the Cassini spacecraft [*Baines et al.*, 2005]. Also, *Kim and Geballe* [2005] constrained the altitude of Saturn's tropospheric haze top by fitting the 3-μm PH_3 absorption depth of their ground-based observation. Nonetheless, extensive studies of this spectral region, where the reflected sunlight still dominates owing to Saturn's low temperature, were hindered by the lack of accurate PH_3 line parameters.

[5] Fortunately, a new set of PH_3 line data over 3-μm region (from 2700 to 3600 cm^{-1}) was recently obtained by *Butler et al.* [2006]. As demonstrated by *Kim and Geballe* [2005], Saturn's 3-μm spectrum is a good indicator of either the upper tropospheric haze altitude at around 0.1–0.6 bar

[1] Jet Propulsion Laboratory, California Institute of Technology, Pasadena, California, USA.
[2] Pittsburg State University, Pittsburg, Kansas, USA.
[3] Laboratoire Inter-Universitaire des Systèmes Atmosphériques, CNRS, Université Paris VII and Paris XII, Créteil, France.

0148-0227/06/2006JE002720$09.00

level [*Muños et al.*, 2004; *Temma et al.*, 2005; *Pérez-Hoyos et al.*, 2005] or the PH_3 abundance above the haze on Saturn. Since present knowledge of PH_3 on Saturn is based mostly on the analyses of the 5–10-μm spectrum, a new detailed study of the 3-μm region will further elucidate the vertical and horizontal PH_3 distribution on Saturn.

[6] However, a well-known difficulty in calculating infrared (IR) or near-infrared (NIR) radiation lies in dealing with densely packed spectral lines. Because of finite spectral resolving power of observational instruments (e.g., spectral resolving power of VIMS IR channel = 50–300), averaging calculated line-by-line (LBL) intensities over a spectrally wide bin is inevitably necessary when one compares model spectra with observations. This often results in a dauntingly large computational burden because sharp crowded lines require a large number of computational nodes for accurate spectral integration within a bin. Typical methods to circumvent this problem are the so-called k distribution and correlated-k methods, which are applied respectively to vertically homogeneous and inhomogeneous atmospheres [*Goody and Yung*, 1989; *Lacis and Oinas*, 1991; *Liou*, 2002]. These approximations enable efficient and accurate numerical simulations on a practical timescale and have proven successful in CH_4 absorption studies of giant planets [e.g., *Irwin et al.*, 1998, 2005]. Unfortunately, those techniques have never been applied to PH_3 bands because the essential "k coefficients" were lacking.

[7] In this paper, we present computational procedures and results of PH_3 exponential sum k coefficients in the PH_3-line-rich 3-μm region for correlated-k exponential sum fit (ESF) methods. When used together with existing CH_4 and NH_3 absorption data, our PH_3 k coefficients will bring us more accurate information than before about spatial distribution of NH_3 and PH_3 on Saturn, by improving the fits between observed and simulated spectra near 3400 cm^{-1} where absorption bands of NH_3 and PH_3 overlap. Extensive application of the current results to detailed radiative transfer analyses of VIMS Saturn spectra will be the main topic of our forthcoming publication. In addition, our results will facilitate the analysis of the data sets of Galileo NIMS and New Horizon's future Jupiter swing-by to study the PH_3 distribution on Jupiter.

2. Data Set and Computational Procedure

[8] The principle of the k distribution or correlated-k method is to divide a certain spectral interval into numerous short subintervals and then rearrange them in the order of their absorption coefficient k. The k distribution function $f(k)$ is defined as

$$f(k)dk = \frac{1}{\nu_2 - \nu_1} \sum_m \Delta\nu_m,$$

where ν_2 and ν_1 are the ends of a certain spectral interval, and $\Delta\nu_m$ is the width of a subinterval within which the absorption coefficient is between k and $k + dk$. Namely, $f(k)dk$ represents the total fraction of spectral interval where the absorption coefficient resides in a range from k to $k + dk$, within a designated spectral bin. Accordingly, we can define a cumulative k distribution function as

$$g(k) \equiv \int_0^k f(k)dk,$$

and we can use the inverse of g(k)

$$k = g^{-1},$$

as an alternative to describe the k distribution within the spectral bin. Since g^{-1} is much smoother than the spectral distribution $k(\nu)$, the corresponding transmission profile along the g ordinate is also smooth enough that the integration in the g space can be well approximated by summing a small number of Gaussian quadrature terms, as later described in this section. More extensive descriptions of this entire procedure are seen elsewhere [e.g., *Goody and Yung*, 1989; *Lacis and Oinas*, 1991; *Liou*, 2002].

[9] To implement this method, we first obtain an exact PH_3 absorption spectrum by LBL absorption over the entire spectral interval of interest. In the present study, we use the recent PH_3 line data between 2.8 and 3.6 μm consisting of accurate room temperature laboratory measurements of ~8000 PH_3 line positions, intensities, and lower state transition energies compiled by *Butler et al.* [2006]. These assignments permit those lines to be properly scaled to corresponding values at other temperatures by ordinary well-known equations. Line positions obtained at 0.011-cm^{-1} resolution on a Fourier Transform Spectrometer were calibrated with the CO wavelength standards at 2.3 μm reported by *Pollock et al.* [1983].

[10] The volume mixing ratios of hydrogen ($\equiv q_{H_2}$) and helium ($\equiv q_{He}$) are assumed to be 0.865 and 0.135, respectively. These numbers are consistent with the newly estimated ranges of Saturn's q_{H_2} and q_{He} [*Conrath and Gautier*, 2000] and match with those of Jupiter measured by the Galileo entry probe [*von Zahn et al.*, 1998]. Therefore our results are readily applicable to both Jupiter and Saturn.

[11] Calculated hydrogen-broadening coefficients for our computation were provided by J.-P. Bouanich (private communication, 2005), on the basis of the room temperature analysis presented by *Bouanich et al.* [2004]. The temperature dependence coefficient n of the hydrogen broadening was obtained from *Salem et al.* [2004] using the expression $n = 0.702 - 0.1 \times J$ (J is the lower state rotational quantum number), and pressure-induced frequency shifts were set to zero. Widths of several hundred forbidden transitions ($\Delta K > 1$), not provided by Bouanich, were estimated using values of corresponding transitions with the same lower state quanta and same values of ΔJ with $\Delta K = 0$ or ± 1 (K is the quantum number of angular momentum along the molecule's symmetry axis). A few dozen high-J lines were also not calculated and so these widths were set to the value corresponding to $J = 22$ at the same K.

[12] To estimate helium-broadening coefficients, we computed the ratio of (helium-broadening coefficient)/(hydrogen-broadening coefficient) for 17 lines by comparing *Bouanich et al.* [2004] and *Salem et al.* [2005] near 10 μm and obtained an average value of 0.52 ± 0.01. On

Table 1. Temperature and Pressure Points Where Our k Coefficients Were Computed

Variable	Values of Sampled Points					
T, K	80	90	100	110	120	130
	140	150	160	170	190	210
	230	250	270	290	310	330
	350					
p, bars	10^{-3}	$10^{-2.75}$	$10^{-2.5}$	$10^{-2.25}$	10^{-2}	$10^{-1.75}$
	$10^{-1.5}$	$10^{-1.25}$	10^{-1}	$10^{-0.75}$	$10^{-0.5}$	$10^{-0.25}$
	10^{0}	$10^{0.25}$	$10^{0.5}$	$10^{0.75}$	10^{1}	

the assumption that the same relation between the hydrogen- and helium-broadening holds in other spectral regions, we used this ratio for the hydrogen-broadening coefficients near 3 μm, to obtain the helium-broadening coefficients.

[13] We ignored self-broadening by PH_3 itself because it is always negligibly small compared with those by hydrogen and helium if the PH_3 volume mixing ratio ($\equiv q_{PH_3}$) is 10^{-5}–10^{-6} or smaller as in the giant planets' atmospheres [e.g., *Courtin et al.*, 1984; *Prinn et al.*, 1984; *Loddars and Fegley*, 1998; *Orton et al.*, 2000; *Atreya et al.*, 2003].

[14] Although the combination of *Butler et al.* [2006] and the newest HITRAN database [*Rothman et al.*, 2005] provided PH_3 line parameters from 770 to 3601 cm^{-1} (2.78–12.99 μm), the k coefficients were computed only over 2750–3550 cm^{-1} (2.82–3.64 μm). This computation cutoff at the large–wave number side was set because no PH_3 line parameters were available when the wave number ν was larger than 3601 cm^{-1}. Consequently, the computational result of the large–wave number end of the data coverage does not account for the wing effects of weak absorption lines lying just outside the spectral data range, especially when the pressure broadening is significant ($p \gtrsim 1$ bar). At the small-wave number end, the computation was not extended further down because of limited computational time and little practical importance of PH_3 line analysis around 2700 cm^{-1} due to far more dominant CH_4 absorption.

[15] In our LBL calculation, we assumed Voigt profile for each line and simple linear summation for line overlapping:

$$k(\nu, p, T) = \frac{1}{\sqrt{\pi}} \sum_l \frac{S_l(T)}{\alpha_{D,l}(T)} V(x_l(\nu, T), y_l(p, T)),$$

where

$$V(x_l, y_l) = \frac{y_l}{\pi} \int_{-\infty}^{+\infty} \frac{e^{-t^2}}{y_l^2 + (x_l - t)^2} dt$$

and

$$x_l \equiv (\nu - \nu_l)/\alpha_{D,l}(T), \quad y_l \equiv \alpha_{D,l}(T)/\alpha_{L,l}(p, T).$$

Here, l is the index of the lth absorption line, $S_l(T)$ is the line strength of the lth absorption line, $\alpha_{D,l}(T)$ is the Doppler width of the lth line, $\alpha_{L,l}(p, T)$ is the Lorentz half width of the lth line, ν_l is the line center wave number of the lth line, ν is the wave number of interest, p is the ambient total atmospheric pressure, and T is the ambient atmospheric temperature. The temperature dependence of line strengths and Lorentz half widths were calculated from the formulae (A11) and (A12) of *Rothman et al.* [1998]. The internal partition sum of PH_3 molecule was interpolated from a data file (parsum.dat) available in the HITRAN 2004 database [*Rothman et al.*, 2005].

[16] With respect to the ambient pressure and temperature in our computation, we simulated the conditions of Jupiter and Saturn in the stratosphere and upper troposphere, throughout the visible regions of these aerosol-laden atmospheres. The minimum temperature near the tropopause of Saturn is about 80 K (about 110 K at Jupiter's tropopause), and the temperature at 10-bar level in Jupiter is about 340 K (about 270 K at the 10-bar level on Saturn). Accordingly, we chose 19 temperatures from 80 to 350 K. The grid points of the ambient atmospheric pressure were evenly sampled on logarithmic scale with an increment factor of $10^{0.25}$, resulting in 17 pressure points from 10^{-3} to 10 bars. These temperature and pressure grid points, presented in Table 1, apply to the vertical range of the giant planets from the relatively deep troposphere to the upper stratosphere. No k coefficients are derived at any pressure lower than 10^{-3} bars because PH_3 is highly depleted above the tropopause ($p \lesssim 0.1$ bar) of both Jupiter and Saturn [*Irwin et al.*, 1998; *Orton et al.*, 2000]. The vertical profiles of T and q_{PH_3} on Jupiter and Saturn are illustrated in Figure 1.

[17] The wing cutoff distance ($\equiv \Delta\nu_{wing}$) of each absorption line and spectral resolution ($\equiv \Delta\nu_{resol}$) for the LBL computation (Table 2) were empirically determined according to the given ambient pressure in order to minimize computational time while the normalization accuracy of each line was always kept within 0.5%.

[18] From the entire absorption coefficient spectrum, we extracted 401 bins of 2-cm^{-1} width with a spectral step of 2 cm^{-1}. This spectral resolution, equivalent to $\Delta\lambda$ = 0.001–0.0015 μm near 3 μm, was chosen to resolve the

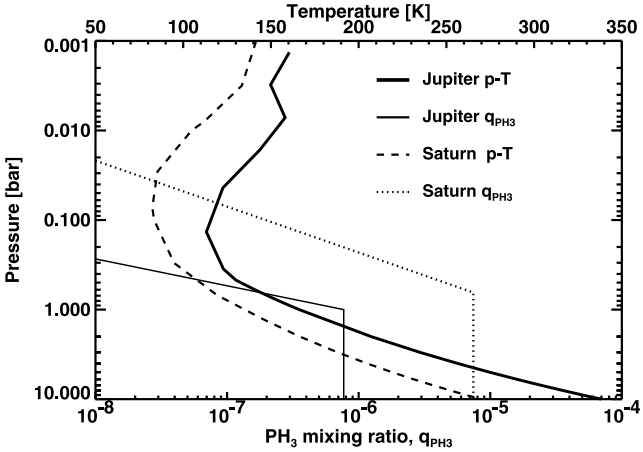

Figure 1. Vertical PH_3 volume mixing ratio ($\equiv q_{PH_3}$) profiles on Jupiter [*Irwin et al.*, 1998] and Saturn [*Orton et al.*, 2000]. The p-T profiles in the Jovian and Saturnian stratospheres and upper tropospheres are overplotted (top scale). Jupiter's temperature data are from the Galileo entry probe at 6.5°N latitude [*Seiff et al.*, 1998]. Saturn's p-T data are from *Lindal et al.* [1985] at 36°N latitude, where we assumed a constant adiabatic lapse rate below the 1.3-bar level.

Table 2. Wing Cutoff Distance and Computational Spectral Resolution Used in Our Line-by-Line Computations at Various Ambient Pressures

Pressure, bars	$\Delta\nu_{wing}$, cm^{-1}	$\Delta\nu_{resol}$, cm^{-1}
10^{-3}	5	10^{-4}
$10^{-2.75}$	5	10^{-4}
$10^{-2.5}$	5	10^{-4}
$10^{-2.25}$	10	2×10^{-4}
10^{-2}	10	2×10^{-4}
$10^{-1.75}$	10	2×10^{-4}
$10^{-1.5}$	10	2×10^{-4}
$10^{-1.25}$	10	2×10^{-4}
10^{-1}	20	10^{-3}
$10^{-0.75}$	40	10^{-3}
$10^{-0.5}$	60	2×10^{-3}
$10^{-0.25}$	80	2×10^{-3}
10^{0}	200	5×10^{-3}
$10^{0.25}$	350	5×10^{-3}
$10^{0.5}$	500	5×10^{-3}
$10^{0.75}$	650	10^{-2}
10^{1}	800	10^{-2}

triangular spectral response across each spectral resolution element of VIMS IR channel ($\Delta\lambda = 0.0166$ μm). In each of those spectral bins, we derived a k distribution $f(k)$ and cumulative k distribution $g(k)$. Then, the exponential sum k coefficients were obtained in the same manner as by *Baines et al.* [1993] and *Irwin et al.* [2005]. Namely, the ith k coefficient k_i was given by the inverse mapping of g as

$$k_i = g^{-1}(g_i),$$

where g_i ($i = 1, 2, \cdots, N$) is the ith node of the N point Gaussian quadrature points along the g ordinate.

[19] Once these k coefficients are acquired, the average transmission in the nth spectral bin ($\equiv \bar{T}^n$) in a uniform atmospheric layer of specific T and p is given by

$$\bar{T}^n = \sum_{i=1}^{N} w_i e^{-k_i^n u},$$

where u is the total column abundance of the absorbing molecule along the optical path in the layer. w_i is the Gaussian weight associated with the ith Gaussian quadrature node and $k_i^n(T, p)$ is the k coefficient of the layer at the nth spectral bin at the ith Gaussian quadrature node. When a vertically inhomogeneous atmosphere is considered, it is divided into a stack of layers having varying T and p, and the bin-averaged transmission down to the mth atmospheric layer ($\equiv \bar{T}_m^n$) is computed as

$$\bar{T}_m^n = \sum_{i=1}^{N} w_i e^{-\sum_{j=1}^{m} k_{ij}^n u_j},$$

where $k_{i,j}^n(T, p)$ and u_j are the quantities of the jth layer. The bin-averaged total absorption optical thickness down to the mth layer ($\equiv \bar{\tau}_m^n$) is derived as

$$\bar{\tau}_m^n = -\ln \bar{T}_m^n.$$

[20] In order to determine the number of quadrature points, we computed and compared the accuracies of 10-, 20- and 40-point cases. Within the pressure range of our data set ($0.001 \leq p \leq 10$ bars), the difference in accuracy among the three cases was negligibly small until PH_3 column abundance ($\equiv u_{PH3}$) reached $\sim$0.1 km amagat. Actually, such high u_{PH3} is hardly encountered in ordinary analyses of the outer planets' atmospheres, as explained in the following section. Therefore we adopted 10-point Gaussian quadrature, considering simplicity and consistency with previous works. The $\{g_i\}$ and $\{w_i\}$ ($i = 1, 2, ..10$) over $0 \leq g \leq 1$ are listed in our k coefficient data file available to the public.

3. Results and Discussion

[21] For brevity and economy of paper space, we present here our computational results only at a spectral bin centered at 3400 cm^{-1}. This sample bin is chosen to study the effects of pressure and temperature variations on the main PH_3 absorption region. The change in the absorption coefficient spectrum with pressure and temperature is shown in Figure 2. As obviously seen, the main influence of an increased pressure is to smooth out the entire absorption spectrum. The variation in temperature also alters the absorption strength by changing population densities of the lower energy states. Consequently, the cumulative k distribution $g(k)$ also varies according to p and T, as presented in Figure 3, resulting in different k coefficients at different (p, T) combinations. The bin-averaged transmission over 3400 ± 1 cm^{-1} and accuracy of the ESF fit are plotted in Figures 4 and 5. Generally, the ESF results start to deviate from those of LBL when PH_3 absorption reduces transmission down to $\sim$0.01. At a certain PH_3 column abundance, the transmission decreases with increasing pressure because the pressure-broadening effect redistributes the absorption of otherwise saturated lines to nearby continuum regions.

[22] Using the obtained k coefficients, the photon penetration depth (depth of $\tau = 1$ along returning nadir path) for Jupiter and Saturn are displayed in Figures 6 and 7, to illustrate how deep we can remotely sense these atmospheres. In the Jovian atmosphere, the existence of PH_3 barely influences the photon penetration limit simply because of the low PH_3 abundance. Contributions by stratospheric molecules like C_2H_2 and C_2H_6 to the total absorption in this spectral region are small and ignored. As seen in Figures 6 and 7, little solar radiation reaches and returns from a depth of $\sim$2 bars in the giant planets because of absorption of various gas species. When extinction by aerosols is also taken into account, this penetration limit altitude becomes even higher. Along a nadir returning optical path down to the 2-bar level, the corresponding u_{PH3} is $\leq 10^{-4}$ and $\sim 2 \times 10^{-3}$ km amagat in Jupiter and Saturn, respectively. With these low u_{PH3} values and pressures lower than 2 bars, the deviation in transmission between LBL and ESF is always smaller than a few percent as presented in Figures 4 and 5. Therefore transmission uncertainty by the use of our k coefficients is unlikely to exceed a few percent in studies of 3-μm solar radiation reflected from the giant planets.

[23] For future spectral analysis, we see in Figures 6 and 7 that the region where $\nu \leq 3200$ cm^{-1} can be used to determine the upper haze layer height by fitting the dominant CH_4 absorption on both planets. Then, the NH_3 column

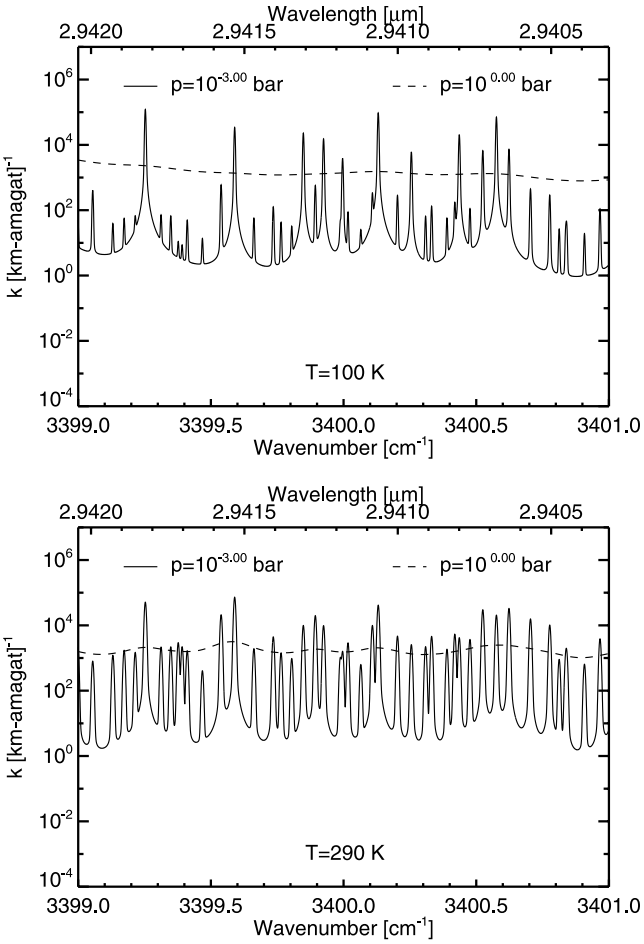

Figure 2. Spectral distribution of PH_3 absorption coefficient k ($\equiv k(\nu)$) over $\nu = 3400 \pm 1$ cm^{-1} at (top) $T = 100$ and (bottom) $T = 290$ K at two different pressures, demonstrating the pressure-broadening effect in a strong PH_3 absorption region.

abundance above the haze layer top is constrained by NH_3 absorption analysis near 3330 cm^{-1} for Saturn, and between 3300 and 3500 cm^{-1} for Jupiter, where NH_3 absorption significantly exceeds that of CH_4 and PH_3. Given knowledge of haze layer tops and NH_3 column abundance obtained by the preceding analyses, the PH_3 column abundance is determined by fitting the spectrum from 3350 to 3500 cm^{-1}, where the PH_3 absorption is the strongest in this 3-μm region. The Cassini VIMS data, which comprise two-dimensional Saturn images over this entire spectral region, would be extremely useful for this entire scheme of spectral study.

[24] Our wing cutoff at low pressures ($p \leq 0.1$ bar) is smaller than that in some previous works [e.g., *Irwin et al.*, 2005]. Examining this influence, making test computations with a wing cutoff of 30 cm^{-1}, we found only marginal difference ($\lesssim$1% in bin-averaged transmission) from our original result, except when u_{PH3} reached about 10^{-2} km amagat. Considering the practical upper limit of u_{PH3} discussed above, the uncertainty caused by our small wing cutoff is less than $\sim$1% and safely neglected.

[25] In contrast, a very large wing cutoff (200–800 cm^{-1}) is necessary to accurately normalize each line at high pressures ($p \geq 1$ bar). This is partly because the hydrogen-broadening coefficients of PH_3 are relatively large (e.g., $\sim$1.5 times those of CH_4 around 3 μm, when the PH_3 line data of *Butler et al.* [2006] are compared with those of CH_4 in work by *Pine* [1992]), but mainly because of the wide Lorentzian wing of Voigt profile. The far-wing contributions of strong lines are prominent at spectral regions of very weak absorption. When $p = 10$ bars, the far-distant wings of some very strong PH_3 lines centered around 2400 cm^{-1} are comparable with the absorption peaks of weak lines near 3000 cm^{-1}. Thus close attention should be paid to wing cutoff size when LBL computations are conducted in weak absorption regions under high pressures with Lorentz or Voigt profiles. Since no general formula exists for the optimum wing cutoff as a function of wave number and line strength, it is determined only by repetitive trial-and-error process, depending on the spectral distribution of line strength and limitation in computational resource.

[26] The demand for a large wing cutoff brings into question the accuracy of our LBL computation near the large–wave number edge of our data coverage under high pressures, because no PH_3 line data are available at

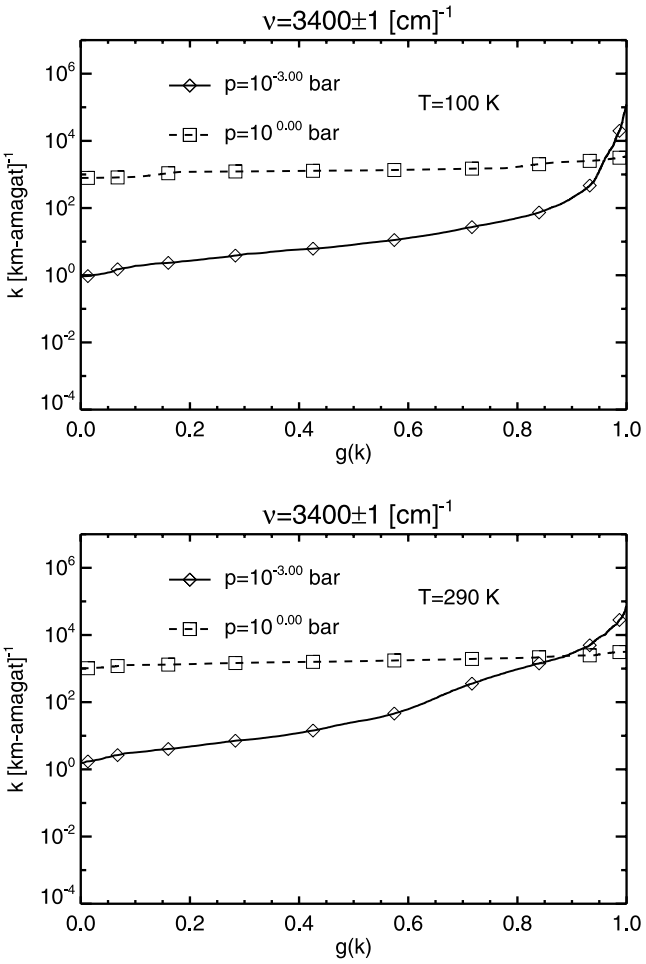

Figure 3. PH_3 absorption coefficient k as a function of cumulative k distribution $g(k)$ at two different pressures with (top) $T = 100$ and (bottom) $T = 290$ K. The symbols denote the positions of k values at the 10-point Gaussian quadrature nodes.

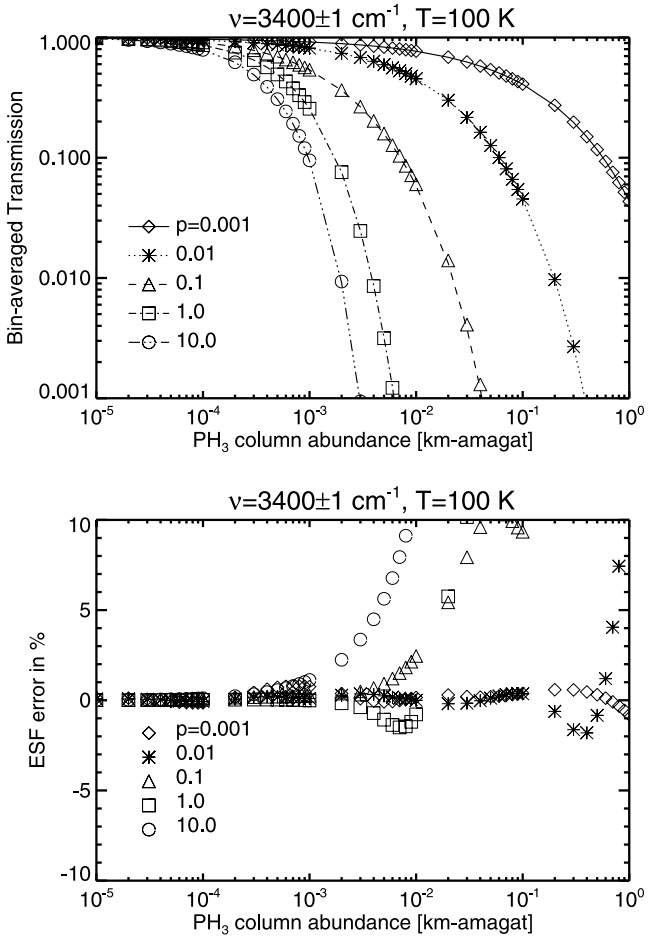

Figure 4. (top) Bin-averaged transmission with $T = 100$ K over $\nu = 3400 \pm 1$ cm^{-1} by LBL (lines) and ESF (symbols) computations at various ambient pressures (p, bars), represented by different line styles and symbols. (bottom) Fractional deviations between LBL and ESF of the top plot. The deviation in % is defined as 100(ESF − LBL)/LBL.

$\nu \geq 3601$ cm^{-1}. Therefore we examine it at 3550 cm^{-1} as follows. We conduct a LBL computation with a wing cutoff of 50 cm^{-1}, considering only the wing effects of the lines located between 3500 and 3600 cm^{-1}. Then, this is compared with our original result, which incorporates the line wing effects between $\nu \leq 3500$ cm^{-1} and 3601 cm^{-1}. Namely, the difference between the above two results represents the line wing effects at 3550 cm^{-1} from the region of $\nu \leq 3500$ cm^{-1}. This comparison demonstrates that the difference in bin-averaged transmission at 3550 cm^{-1}, which increases with increasing u_{PH3}, is smaller than 1–2% if $u_{PH3} \lesssim 2 \times 10^{-3}$ km amagat at $p \lesssim 2$ bars. In view of the previously mentioned solar photons' penetration depth and our laboratory measurements indicating that PH_3 lines at $\nu \geq 3600$ cm^{-1} are much weaker than those at $\nu \leq 3500$ cm^{-1}, we can reasonably say that the transmission uncertainty near 3550 cm^{-1} due to the lack of the large–wave number region data ($\nu \geq 3601$ cm^{-1}) does not exceed a few percent in studying reflected sunlight from the giant planets.

[27] Our computational spectral resolution at relatively high pressures ($p \gtrsim 1$ bar) is somewhat cruder than in some previously published works (e.g., $\Delta\nu_{resol} = 10^{-3}$ in the work by *Irwin et al.* [1996]). Nevertheless, another set of computations at $p = 1$ and 10 bars demonstrates that the deviation in bin-averaged transmission between $\Delta\nu_{resol} = 10^{-3}$ and $\Delta\nu_{resol} = 5 \times 10^{-3}$ or 10^{-2} cases is negligibly small ($\lesssim$1%), until the transmission itself diminishes down to 10^{-2} or less. Therefore our computational spectral resolution at high pressures is still fine enough to maintain sufficient computational accuracy in most practical analyses.

[28] *Irwin et al.* [2001] suggested existence of an unknown substance in Jupiter's atmosphere to account for the anomalous absorption over the spectral range from 2.9 to 3.2 μm (from 3125 to 3448 cm^{-1}), which resembled the relatively flat absorption spectrum of NH_3 gas. According to *Butler et al.* [2006], PH_3 absorption is strong near 3430 cm^{-1} ($\lambda \sim 2.9$ μm) and rapidly weakens around $\nu \lesssim 3300$ cm^{-1} ($\lambda \gtrsim 3$ μm). Therefore, if PH_3 is responsible for the flat anomalous absorption spectrum, there needs to be another material that compensates for the weak PH_3 absorption over $\lambda \gtrsim 3$ μm. Absorption by stratospheric C_2H_6 exists near 3.1 μm, but this is unlikely to contribute significantly because of the low C_2H_6 column abundance ($3.0 \pm 1.4 \times 10^{-5}$ km amagat by *Bjoraker et al.* [1981]). Another possible cause of the anomaly is the underestimated NH_3 absorption in the data set adopted by *Irwin et al.* [2001]. In fact, there are some discrepancies among different NH_3 k coefficient data sets from different

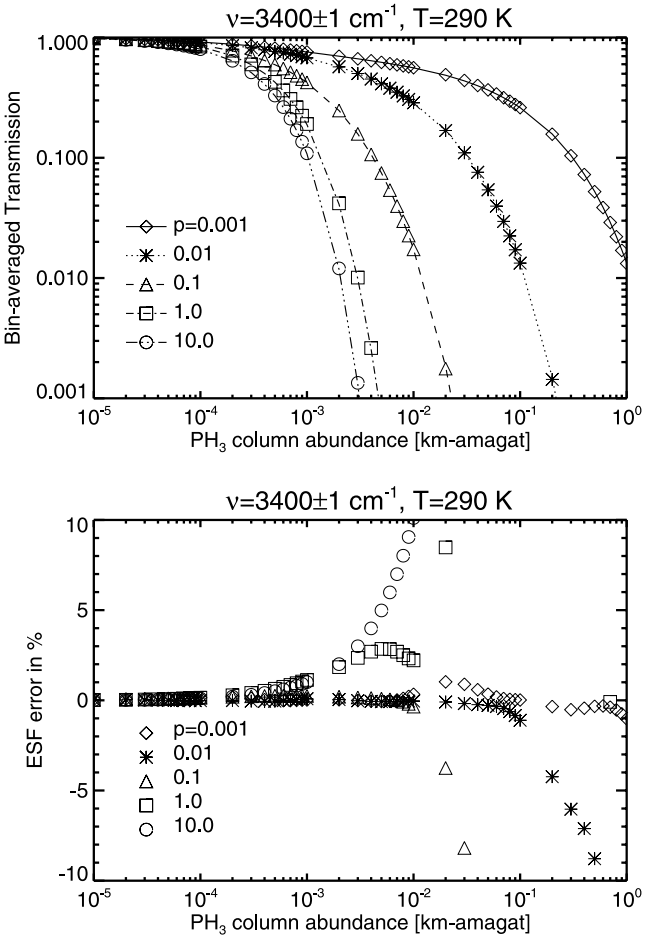

Figure 5. Same as Figure 4, except with $T = 290$ K.

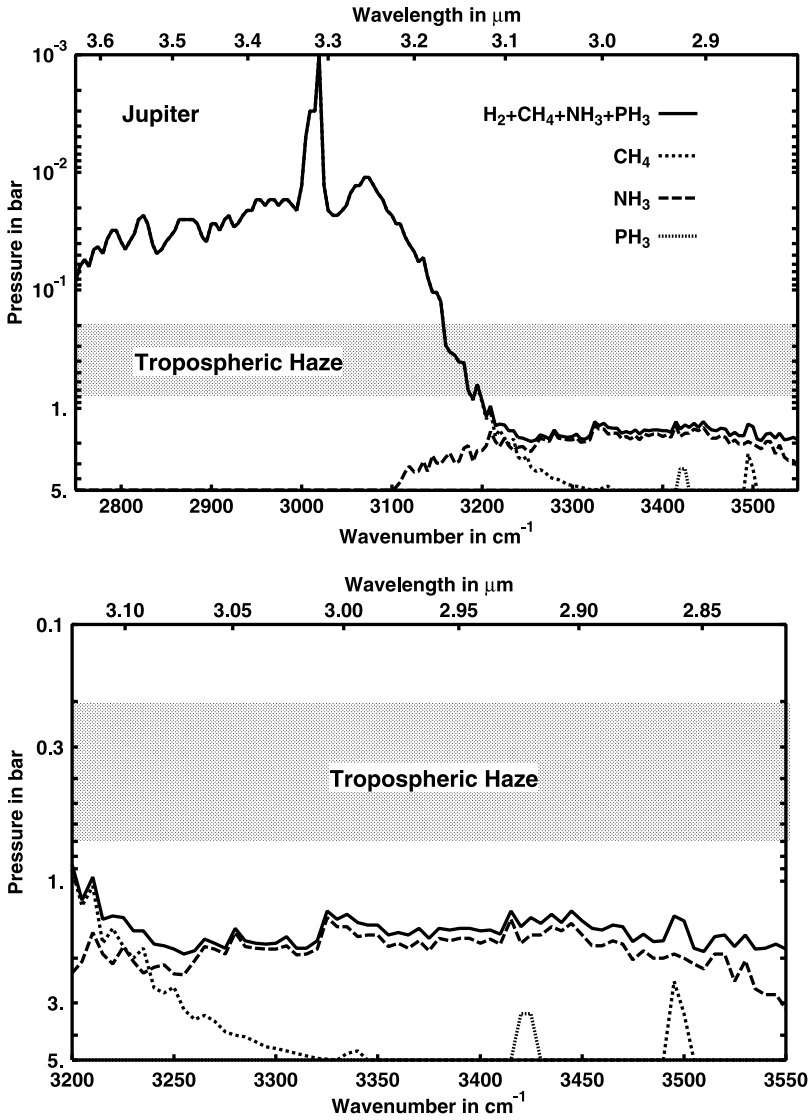

Figure 6. Altitude of $\tau = 1$ along a returning nadir path ($\tau = 0.5$ along a one-way nadir path) in Jupiter when an aerosol-free atmosphere is assumed. The bottom plot, where the legends are same as in the top plot, is the close-up of the 3200–3550 cm^{-1} region where absorption by NH_3 and PH_3 becomes comparable with or stronger than that of CH_4. The H_2 collision-induced absorption opacity was computed from the tabulation of *Borysow* [1991]. The CH_4 k data were taken from *Irwin et al.* [2005]. The NH_3 k values, which are based on the NH_3 line data of *Kleiner et al.* [1999], were provided by P. G. J. Irwin (private communication, 2006). The H_2 collision-induced absorption is insignificant in this spectral region. The vertical NH_3 and PH_3 mixing ratio profiles were adopted from *de Pater and Massie* [1985] and *Irwin et al.* [1998], respectively. The CH_4 mixing ratio was assumed to be 0.002 throughout the Jovian atmosphere [*de Pater and Lissauer* 2001]. The shaded areas indicate the altitude range where the upper tropospheric haze exists in Jupiter's equatorial region [*West et al.*, 2004].

sources. If the anomaly resulted from this underestimated absorption, the spectral similarity between NH_3 gas and the unknown absorber would be readily explained. Thus we point out two possibilities for the anomaly reported by *Irwin et al.* [2001]: (1) PH_3 is partly responsible for the anomalous 3-μm absorption, but another substance absorbing at $\lambda \sim 3$ μm is left undetermined, (2) the anomaly was caused by the underestimated NH_3 gas absorption in the k coefficients used by *Irwin et al.* [2001]. Quantitative examinations of these possibilities are out of the scope of our work but would be worth carrying out in future.

[29] Finally, we mention the line-mixing effect and uncertainty in our PH_3 line parameters. The line mixing is unfortunately uncharacterized for PH_3 lines. It is known to significantly reduce the far-wing absorption of CH_4 lines [e.g., *Hartmann et al.*, 2002; *Tran et al.*, 2006a, 2006b]. If it behaves similarly for PH_3 lines, our PH_3 k coefficient values could significantly overestimate the weak PH_3 absorption around 3000 cm^{-1}, while those of the major absorption region near 3400 cm^{-1} might remain relatively unaffected. Also, uncertainties in some of our PH_3 line parameters are still not well specified. These two factors leave room for

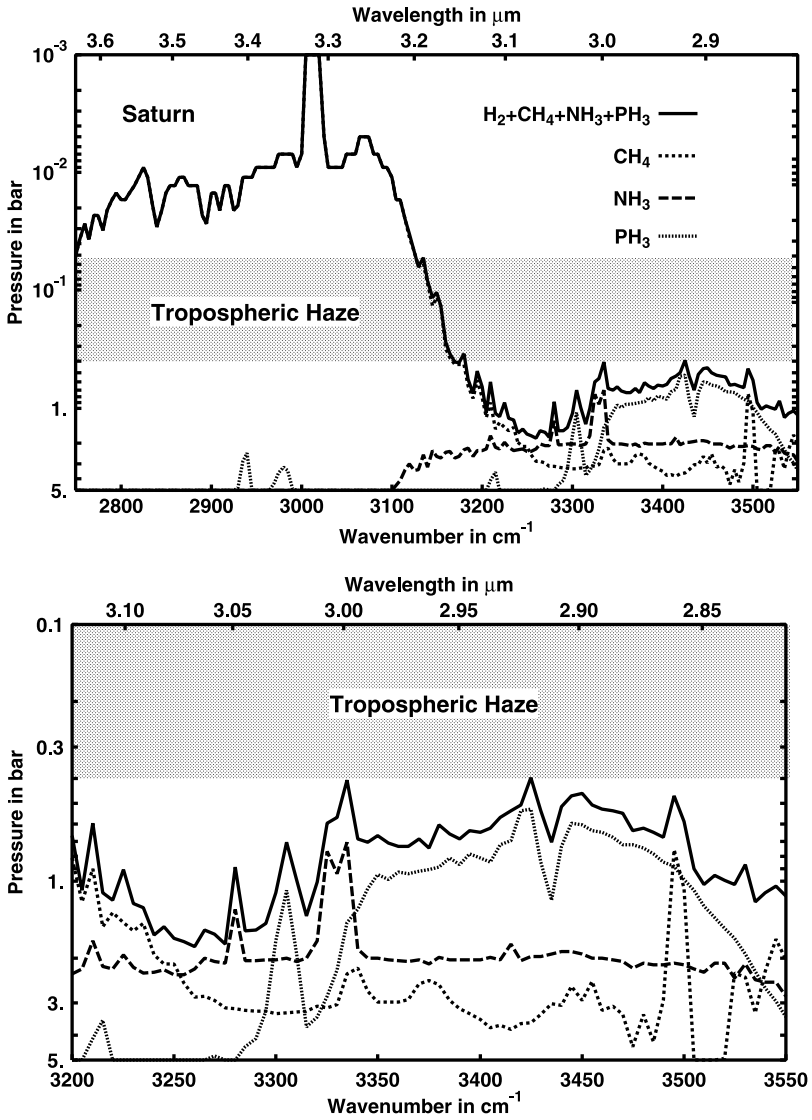

Figure 7. Same as Figure 6 but for Saturn. The vertical NH_3 and PH_3 mixing ratio profiles were adopted from *de Pater and Massie* [1985] and *Orton et al.* [2000], respectively. We assumed a CH_4 mixing ratio of 0.004 throughout the Saturnian atmosphere [*de Pater and Lissauer* 2001]. The vertical range of the upper tropospheric haze roughly indicates the vertical range where the layer was found by the recent visible methane band analyses [*Muños et al.*, 2004; *Temma et al.*, 2005; *Pérez-Hoyos et al.*, 2005] in Saturn's equatorial region.

further improvements in the 3-μm PH_3 k coefficients in future, but our current data set will suffice to serve the purpose of studying the strong 3-μm PH_3 band observed on Saturn with Cassini VIMS.

4. Summary

[30] PH_3 exponential sum k coefficients were obtained between 2750 and 3550 cm^{-1}, with a spectral bin width of 2 cm^{-1} and a spectral step of 2 cm^{-1}. This data set will be useful for radiative transfer analyses of 3-μm observations of Jupiter and Saturn, acquired by Galileo NIMS, ongoing Cassini VIMS, and the future New Horizons space probe during its Jupiter swing-by. Mapping the horizontal and vertical distribution of PH_3 molecules on the giant planets will reveal the three-dimensional nature of their global circulation, including spatial variability of vertical transport from deep interiors of their dynamic atmospheres. Also, we note that a very large wing cutoff is necessary for line-by-line computations under high pressures when Lorentz or Voigt line shapes are assumed. Future inclusion of line-mixing effects could result in smaller k coefficients than ours at weak PH_3 bands. Our PH_3 k coefficient data, compiled in a text file "ph3_kdata_3micron.txt" (20 MB size), can be acquired from the Web site of the NASA Planetary Data System Atmospheres Node, http://atmos.nmsu.edu/.

[31] **Acknowledgments.** We greatly thank P. G. J. Irwin and N. Bowles of Oxford University for kindly providing their NH_3 data for our examination of NH_3 k coefficients. Also, we appreciate the constructive comments from P. G. J. Irwin and an anonymous reviewer. This research was carried out by the Jet Propulsion Laboratory, California Institute of Technology,

under a contract with the National Aeronautics and Space Administration. This work was partly supported by the Research Associateship Award of the National Research Council (transferred to NASA Postdoctoral Fellowship of the Oak Ridge Associated Universities since 1 January 2006) at the Jet Propulsion Laboratory.

References

Atreya, S. K., M. H. Wong, T. C. Owen, P. R. Mahaffy, H. B. Niemann, I. de Pater, P. Drossart, and T. Encrenaz (1999), A comparison of the atmospheres of Jupiter and Saturn: Deep atmospheric composition, cloud structure, vertical mixing, and origin, *Planet. Space Sci.*, *47*, 1243–1262.

Atreya, S. K., P. R. Mahaffy, H. B. Niemann, M. H. Wong, and T. C. Owen (2003), Composition and origin of the atmospheres of Jupiter—An update, and implications for the extrasolar giant planets, *Planet. Space Sci.*, *51*, 105–112.

Baines, K. H., R. A. West, L. P. Giver, and F. Moreno (1993), Quasi-random narrow-band model fits to near-infrared low-temperature laboratory methane spectra and derived exponential-sum absorption coefficients, *J. Geophys. Res.*, *98*(E3), 5517–5529.

Baines, K. H., et al. (2005), The atmospheres of Saturn and Titan in the near-infrared: First results of Cassini/VIMS, *Earth Moon Planets*, *96*, 119–147.

Bjoraker, G. L., H. P. Larson, U. Fink, and H. A. Smith (1981), A study of ethane on Saturn in the 3 micron region, *Astrophys. J.*, *248*, 856–862.

Bjoraker, G. L., H. P. Larson, and V. Kunde (1986), The gas composition of Jupiter derived from 5 micron airborne spectroscopic observations, *Icarus*, *66*, 579–609.

Borysow, A. (1991), Modeling of collision-induced infrared absorption spectra of H_2-H_2 pairs in the fundamental band at temperatures from 20 to 300 K, *Icarus*, *92*, 273–279.

Bouanich, J. P., J. Salem, H. Aroui, J. Walrand, and G. Blanquet (2004), H2-broadening coefficients in the ν_2 and ν_4 bands of PH_3, *J. Quant. Spectrosc. Radiat. Transfer*, *84*, 195–205.

Bregman, J. D., D. F. Lester, and D. M. Rank (1975), Observation of the ν_2 band of PH_3 in the atmosphere of Saturn, *Astrophys. J.*, *202*, L55–L56.

Butler, R. A. H., L. Sagui, I. Kleiner, and L. R. Brown (2006), The absorption spectrum of phosphine (PH_3) between 2.8 and 3.7 μm: Line positions, intensities, assignments and single state fits, *J. Mol. Spectrosc.*, *238*, 178–192.

Carlson, B. E., A. A. Lacis, and W. B. Rossow (1993), Tropospheric gas composition and cloud structure of the Jovian north equatorial belt, *J. Geophys. Res.*, *98*(E3), 5251–5290.

Conrath, B. J., and D. Gautier (2000), Saturn helium abundance: A reanalysis of Voyager measurements, *Icarus*, *144*, 124–134.

Courtin, R., D. Gautier, A. Marten, B. Bézard, and R. Hanel (1984), The composition of Saturn's atmosphere at northern temperate latitudes from *Voyager* IRIS spectra: NH_3, PH_3, C_2H_2, C_2H_6, CH_3D, CH_4, and the Saturnian D/H isotopic ratio, *Astrophys. J.*, *287*, 899–916.

de Pater, I., and J. J. Lissauer (2001), *Planetary Sciences*, Cambridge Univ. Press, New York.

de Pater, I., and S. T. Massie (1985), Models of the millimeter-centimeter spectra of the giant planets, *Icarus*, *62*, 143–171.

Encrenaz, T. (2004), Neutral atmospheres of the giant planets: An overview of composition measurements, *Space Sci. Rev.*, *116*, 99–119.

Gillett, F. C., and W. J. Forrest (1974), The 7.5- to 13.5-micron spectrum of Jupiter, *Astrophys. J.*, *187*, L37–L39.

Goody, R. M., and Y. L. Yung (1989), *Atmospheric Radiation*, Oxford Univ. Press, New York.

Hartmann, J.-M., C. Boulet, C. Brodbeck, N. van Thanh, T. Fouchet, and P. Drossart (2002), A far wing lineshape for H_2 broadened CH_4 infrared transitions, *J. Quant. Spectrosc. Radiat. Transfer*, *72*, 117–122.

Irwin, P. G. J., S. B. Calcutt, F. W. Taylor, and A. L. Weir (1996), Calculated *k* distribution coefficients for hydrogen- and self-broadened methane in the range 2000–9500 cm^{-1} from exponential sum fitting to band-modelled spectra, *J. Geophys. Res.*, *101*(E11), 26,137–26,154.

Irwin, P. G. J., et al. (1998), Cloud structure and atmospheric composition of Jupiter retrieved from Galileo near-infrared mapping spectrometer real-time spectra, *J. Geophys. Res.*, *103*(E10), 23,001–23,021.

Irwin, P. G. J., A. L. Weir, F. W. Taylor, and S. B. Calcutt (2001), The origin of belt/zone contrasts in the atmosphere of Jupiter and their correlation with 5-μm opacity, *Icarus*, *149*, 397–415.

Irwin, P. G. J., P. Parrish, T. Fouchet, S. B. Calcutt, F. W. Taylor, A. A. Simon-Miller, and C. A. Nixon (2004), Retrievals of Jovian tropospheric phosphine from Cassini/CIRS, *Icarus*, *173*, 84–99.

Irwin, P. G. J., K. Sihra, N. Bowles, F. W. Taylor, and S. B. Calcutt (2005), Methane absorption in the atmosphere of Jupiter from 1800 to 9500 cm^{-1} and implications for vertical cloud structure, *Icarus*, *176*, 255–271.

Kim, S. J., and T. R. Geballe (2005), The 2.9–4.2 micron spectrum of Saturn: Clouds and CH_4, PH_3, and NH_3, *Icarus*, *179*, 449–458.

Kleiner, I., L. R. Brown, G. Tarrago, Q.-L. Kou, N. Picqué, G. Guelachvili, V. Dana, and J.-Y. Mandin (1999), Positions and intensities in the $2\nu_4/\nu_1/\nu_3$ vibrational system of $^{14}NH_3$ near 3 μm, *J. Mol. Spectrosc.*, *193*, 46–71.

Kunde, V., R. Hanel, W. Maguire, D. Gautier, J. P. Baluteau, A. Marten, A. Chedin, N. Husson, and N. Scott (1982), The tropospheric gas composition of Jupiter's north equatorial belt (NH_3, PH_3, CH_3D, GeH_4, H_2O) and the Jovian D/H isotopic ratio, *Astrophys. J.*, *263*, 443–467.

Lacis, A. A., and V. Oinas (1991), A description of the correlated k distribution method for modeling nongray gaseous absorption, thermal emission, and multiple scattering in vertically inhomogeneous atmospheres, *J. Geophys. Res.*, *96*(D5), 9027–9063.

Larson, H. P., R. R. Treffers, and U. Fink (1977), Phosphine in Jupiter's atmosphere—The evidence from high-altitude observations at 5 micrometers, *Astrophys. J.*, *211*, 972–979.

Larson, H. P., U. Fink, H. A. Smith, and D. S. Davis (1980), The middle-infrared spectrum of Saturn: Evidence for phosphine and upper limits to other trace atmospheric constituents, *Astrophys. J.*, *240*, 327–337.

Lindal, G. F., D. N. Sweetnam, and V. R. Eshleman (1985), The atmosphere of Saturn: An analysis of the Voyager radio occultation measurements, *Astron. J.*, *90*, 1136–1146.

Liou, K. N. (2002), *An Introduction to Atmospheric Radiation*, Elsevier, New York.

Loddars, K., and B. Fegley (1998), *The Planetary Scientist's Companion*, Oxford Univ. Press, New York.

Muñoz, O., F. Moreno, A. Molina, D. Grodent, J. C. Gérard, and V. Dols (2004), Study of the vertical structure of Saturn's atmosphere using HST/WFPC2 images, *Icarus*, *169*, 413–428.

Noll, K. S., and H. P. Larson (1990), The spectrum of Saturn from 1990 to 2230 cm^{-1}: Abundances of AsH_3, CH_3D, CO, GeH_4, NH_3, and PH_3, *Icarus*, *89*, 168–189.

Orton, G. S., E. Serabyn, and Y. T. Lee (2000), Vertical distribution of PH_3 in Saturn from observations of its 1-0 and 3-2 rotational lines, *Icarus*, *146*, 48–59, (Correction, *Icarus*, *149*, 489–490, 2001.)

Pérez-Hoyos, S., A. Sánchez-Lavega, R. G. French, and J. F. Rojas (2005), Saturn's cloud structure and temporal evolution from ten years of Hubble Space Telescope images (1994–2003), *Icarus*, *176*, 155–174.

Pine, A. S. (1992), Self-, N_2, O_2, H_2, Ar, and He broadening in the ν_3 band *Q* branch of CH_4, *J. Chem. Phys.*, *97*, 773–785.

Pollock, C. R., F. R. Petersen, D. A. Jennings, J. S. Wells, and A. G. Maki (1983), Absolute frequency measurements of the 2-0 band of CO at 2.3 μm using color center laser spectroscopy, *J. Mol. Spectrosc.*, *99*, 357–368.

Prinn, R. G., H. P. Larson, J. H. Caldwell, and D. Gautier (1984), Composition and chemistry of Saturn's atmosphere, in *Saturn*, edited by T. Gehrels and M. S. Matthews, pp. 88–149, Univ. of Ariz. Press, Tucson.

Ridgway, S. T. (1974), The infrared spectrum of Jupiter, 750–1200 cm^{-1}, *Bull. Am. Astron. Soc.*, *6*, 376.

Ridgway, S. T., L. Wallace, and G. R. Smith (1976), The 800–1200 inverse centimeter absorption spectrum of Jupiter, *Astrophys. J.*, *207*, 1002–1006.

Rothman, L. S., et al. (1998), The HITRAN molecular spectroscopic database and HAWKS (HITRAN Atmospheric Workstation): 1996 edition, *J. Quant. Spectrosc. Radiat. Transfer*, *60*, 665–710.

Rothman, L. S., et al. (2005), The HITRAN 2004 molecular spectroscopic database, *J. Quant. Spectrosc. Radiat. Transfer*, *96*, 139–204.

Salem, J., J. P. Bouanich, J. Walrand, H. Aroui, and G. Blanquet (2004), Hydrogen line broadening in the ν_2 and ν_4 bands of phosphine at low temperature, *J. Mol. Spectrosc.*, *228*, 23–30.

Salem, J., J. P. Bouanich, J. Walrand, H. Aroui, and G. Blanquet (2005), Helium- and argon-broadening coefficients of phosphine lines in the ν_2 and ν_4 bands, *J. Mol. Spectrosc.*, *232*, 247–254.

Seiff, A., D. B. Kirk, T. C. D. Knight, R. E. Young, J. D. Mihalov, L. A. Young, F. S. Milos, G. Schubert, R. C. Blanchard, and D. Atkinson (1998), Thermal structure of Jupiter's atmosphere near the edge of a 5-μm hot spot in the north equatorial belt, *J. Geophys. Res.*, *103*(E10), 22,857–22,889.

Temma, T., N. J. Chanover, A. A. Simon-Miller, D. A. Glenar, J. J. Hillman, and D. M. Kuehn (2005), Vertical structure modeling of Saturn's equatorial region using high spectral resolution imaging, *Icarus*, *175*, 464–489.

Tokunaga, A. T., H. L. Dinerstein, D. F. Lester, and D. M. Rank (1980), The phosphine abundance on Saturn derived from new 10-micrometer spectra, *Icarus*, *42*, 79–85, (Correction, *Icarus*, *48*, 540, 1981.)

Tran, H., P.-M. Fraud, T. Gabard, F. Hase, T. von Clarmann, C. Camy-Peyret, S. Payan, and J.-M. Hartmann (2006a), Model, software and database for line-mixing effects in the ν_3 and ν_4 bands of CH_4 and tests using laboratory and planetary measurements—I: N_2 (and air) broadenings and the Earth atmosphere, *J. Quant. Spectrosc. Radiat. Transfer*, *101*, 284–305.

Tran, H., P.-M. Fraud, T. Fouchet, T. Gabard, and J.-M. Hartmann (2006b), Model, software and database for line-mixing effects in the ν_3 and ν_4 bands of CH_4 and tests using laboratory and planetary measurements—II: H_2 (and He) broadening and the atmospheres of Jupiter and Saturn, *J. Quant. Spectrosc. Radiat. Transfer*, *101*, 306–324.

von Zahn, U., D. M. Hunten, and G. Lehmacher (1998), Helium in Jupiter's atmosphere: Results from the Galileo probe helium interferometer experiment, *J. Geophys. Res.*, *103*(E10), 22,815–22,829.

West, R., K. H. Baines, J. Friedson, D. Banfield, B. Ragent, and F. W. Taylor (2004), Jovian clouds and haze, in *Jupiter*, edited by F. Bagenal, T. Dowling, and W. McKinnon, pp. 79–104, Cambridge Univ. Press, New York.

K. H. Baines, L. R. Brown, R. A. H. Butler, and T. Temma, Jet Propulsion Laboratory, California Institute of Technology, 4800 Oak Grove Drive, Pasadena, CA 91109, USA. (ttemma@scn.jpl.nasa.gov)

I. Kleiner and L. Sagui, Laboratoire Inter-Universitaire des Systèmes Atmosphériques, CNRS, Université Paris VII and Paris XII, 61 av. Général de Gaulle, F-94010 Créteil, France.